arXiv:hep-ph/9811435v1 23 Nov 1998

TIT/HEP-406/NP
November, 1998

Hyperon Non-leptonic Weak Decays in the Chiral Perturbation Theory II

K. Takayama and M. Oka

Department of Physics, Tokyo Institute of Technology
Meguro, Tokyo 152, Japan

Hyperon non-leptonic weak decay amplitudes are studied in the chiral perturbation theory. The weak interaction vertices caused by the four quark operators are substituted by the products of the hadronic currents and by the phenomenologically introduced weak Hamiltonian of hadron operators. Our study suggests the improvement of the theoretical prediction for the weak decay amplitudes.

1. Introduction

The chiral perturbation theory is applied to many hadron phenomena, and succeed to reproduce the experimental data. This theory is applied to the analysis of hyperon non-leptonic weak decays. But this theory cannot reproduce the experimental data[1,2]. In the previous paper[3], we use the chiral perturbation theory as the non-perturbative QCD correction for the weak interaction. The quark four point vertices are substituted by the product of the hadron currents which is derived by the chiral perturbation theory. We can reproduce the suppression of the $\Delta I = 3/2$ amplitudes. But this method cannot reproduce the $\Delta I = 1/2$ amplitudes. It suggests that the product of the hadron currents cannot reproduce all the four point vertices of the quark operators. In this study, we construct the effective weak Hamiltonian which cannot be represented by the product of the hadron currents, and consider the role of the effective Hamiltonian.

This paper is organized as follows. In section 2 we construct the effective weak Hamiltonian. Section 3 presents the numerical analysis and discussion on the hyperon non-leptonic weak decay amplitudes. Section 4 concludes the paper with the comment on the effective weak Hamiltonian using the chiral perturbation theory.

2. The effective weak Hamiltonian

2.1. The current-current interaction

In order to apply the standard theory to the hyperon non-leptonic weak decay, the momentum transfer scale of the weak interaction vertex is changed with the renormalization group method. This method constructs the effective weak Hamiltonian including the perturbative QCD correction to the weak interaction[4,5]. This Hamiltonian is represented by the four point vertices of the quark operator.

Applying the four quark vertex to the hyperon non-leptonic weak decay, we can derive two types of the diagrams, which are shown in Fig. 2.1. In order to derive the effective weak Hamiltonian with the chiral perturbation theory, the quark lines, which have color index, are substituted by the hadron operators which are color singlet. The diagram in Fig. 2.1(a) can be substituted by the product of the hadron currents, but the diagram in Fig. 2.1(b) cannot be represented by it. For the construction of the effective weak Hamiltonian of the diagram in Fig. 2.1(b), we introduce the two ansatz.

1. Applying Fierz transformation to the diagrams in Fig. 2.1, the diagram (b) is changed to the product of the color singlet quark currents. And this product is substituted by the product of the hadron currents.
2. For the residual effect of the ansatz 1, we introduce the phenomenological effective weak Hamiltonian which has parameters.

In the following, the effective weak Hamiltonian described by the product of the hadron currents is called as the current-current interaction, and the effective weak Hamiltonian derived by the ansatz 2 is called as the internal interaction.

Using the above ansatz and the heavy baryon formalism of the chiral perturbation theory, the effective weak Hamiltonian is given by

$$\mathcal{H}_{eff}^{\Delta S=1} = \mathcal{H}_{current}^{\Delta S=1} + \mathcal{H}_{int}^{\Delta S=1} \tag{2.1}$$

$$\mathcal{H}_{current}^{\Delta S=1} = -\frac{G_f}{\sqrt{2}} \sum_{r=1}^{6} K_r O_r, \tag{2.2}$$

where the coefficients K_r is shown in Table 2.1. The operators O_r are given by

$$\begin{aligned}
O_1 &= \tfrac{2}{3}\left(\mathcal{J}_{L\mu}^{23}\mathcal{J}_L^{11\mu} - \mathcal{J}_{L\mu}^{13}\mathcal{J}_L^{21\mu}\right) \\
O_2 &= \tfrac{4}{3}\left(\mathcal{J}_{L\mu}^{23}\mathcal{J}_L^{11\mu} + \mathcal{J}_{L\mu}^{13}\mathcal{J}_L^{21\mu} + 2\mathcal{J}_{L\mu}^{23}\mathcal{J}_L^{22\mu} + 2\mathcal{J}_{L\mu}^{23}\mathcal{J}_L^{33\mu}\right) \\
O_3 &= O_3\left(\Delta I = 1/2\right) \\
&= \tfrac{4}{9}\left(\mathcal{J}_{L\mu}^{23}\mathcal{J}_L^{11\mu} + \mathcal{J}_{L\mu}^{13}\mathcal{J}_L^{21\mu} + 2\mathcal{J}_{L\mu}^{23}\mathcal{J}_L^{22\mu} - 3\mathcal{J}_{L\mu}^{23}\mathcal{J}_L^{33\mu}\right) \\
O_4 &= O_3\left(\Delta I = 3/2\right) \\
&= \tfrac{20}{9}\left(\mathcal{J}_{L\mu}^{23}\mathcal{J}_L^{11\mu} + \mathcal{J}_{L\mu}^{13}\mathcal{J}_L^{21\mu} - \mathcal{J}_{L\mu}^{21}\mathcal{J}_L^{22\mu}\right) \\
O_5 &= O_{51} + O_{52} + O_{53} \\
& \quad O_{51} = \left(\mathcal{J}_{L\mu}^{23}\mathcal{J}_R^{11\mu} + \mathcal{J}_{L\mu}^{23}\mathcal{J}_R^{22\mu} + \mathcal{J}_{L\mu}^{23}\mathcal{J}_R^{33\mu}\right) \\
& \quad O_{52} = -\tfrac{2}{3}\left(\mathcal{J}_{0(S+iP)}^{21}\mathcal{J}_{0(S-iP)}^{13} + \mathcal{J}_{0(S+iP)}^{22}\mathcal{J}_{0(S-iP)}^{23} + \mathcal{J}_{0(S+iP)}^{23}\mathcal{J}_{0(S-iP)}^{33}\right) \\
& \quad O_{53} = -\tfrac{2}{3}\left(\mathcal{J}_{2(S+iP)}^{21}\mathcal{J}_{0(S-iP)}^{13} + \mathcal{J}_{0(S+iP)}^{21}\mathcal{J}_{2(S-iP)}^{13} + \mathcal{J}_{2(S+iP)}^{22}\mathcal{J}_{0(S-iP)}^{23}\right. \\
& \qquad\qquad \left. + \mathcal{J}_{0(S+iP)}^{22}\mathcal{J}_{2(S-iP)}^{23} + \mathcal{J}_{2(S+iP)}^{23}\mathcal{J}_{0(S-iP)}^{33} + \mathcal{J}_{0(S+iP)}^{23}\mathcal{J}_{2(S-iP)}^{33}\right) \\
O_6 &= O_{61} + O_{62} \\
& \quad O_{61} = -\tfrac{32}{9}\left(\mathcal{J}_{0(S+iP)}^{21}\mathcal{J}_{0(S-iP)}^{13} + \mathcal{J}_{0(S+iP)}^{22}\mathcal{J}_{0(S-iP)}^{23} + \mathcal{J}_{0(S+iP)}^{23}\mathcal{J}_{0(S-iP)}^{33}\right) \\
& \quad O_{62} = -\tfrac{32}{9}\left(\mathcal{J}_{2(S+iP)}^{21}\mathcal{J}_{0(S-iP)}^{13} + \mathcal{J}_{0(S+iP)}^{21}\mathcal{J}_{2(S-iP)}^{13} + \mathcal{J}_{2(S+iP)}^{22}\mathcal{J}_{0(S-iP)}^{23}\right. \\
& \qquad\qquad \left. + \mathcal{J}_{0(S+iP)}^{22}\mathcal{J}_{2(S-iP)}^{23} + \mathcal{J}_{2(S+iP)}^{23}\mathcal{J}_{0(S-iP)}^{33} + \mathcal{J}_{0(S+iP)}^{23}\mathcal{J}_{2(S-iP)}^{33}\right)
\end{aligned} \tag{2.3}$$

$$\begin{aligned}
\mathcal{J}_{L\mu}^{ij} &= \mathrm{Tr} v_\mu \bar{B}_v \left[\xi^\dagger h_{ij}\xi, B_v\right] - 2D\mathrm{Tr}\bar{B}_v S_{v\mu}\left\{\xi^\dagger h_{ij}\xi, B_v\right\} \\
&\quad -2F\mathrm{Tr}\bar{B}_v S_{v\mu}\left[\xi^\dagger h_{ij}\xi, B_v\right] \\
&\quad -v_\mu \bar{T}_v^\nu \left(\xi^\dagger h_{ij}\xi\right) T_{v\nu} - 2\mathcal{H}\bar{T}_v^\nu S_{v\mu}\left(\xi^\dagger h_{ij}\xi\right) T_{v\nu} \\
&\quad -2\mathcal{C}\left(\bar{T}_{v\mu}\left(\xi^\dagger h_{ij}\xi\right) B_v + \bar{B}_v\left(\xi^\dagger h_{ij}\xi\right) T_{v\mu}\right) \\
&\quad +if_\pi^2 \mathrm{Tr}\left(h_{ij}(\partial_\mu \Sigma)\Sigma^\dagger\right),
\end{aligned} \tag{2.4}$$

$$\begin{aligned}
\mathcal{J}_{R\mu}^{ij} &= \mathrm{Tr} v_\mu \bar{B}_v \left[\xi h_{ij}\xi^\dagger, B_v\right] + 2D\mathrm{Tr}\bar{B}_v S_{v\mu}\left\{\xi h_{ij}\xi^\dagger, B_v\right\} \\
&\quad +2F\mathrm{Tr}\bar{B}_v S_{v\mu}\left[\xi h_{ij}\xi^\dagger, B_v\right] \\
&\quad -v_\mu \bar{T}_v^\nu \left(\xi h_{ij}\xi^\dagger\right) T_{v\nu} + 2\mathcal{H}\bar{T}_v^\nu S_{v\mu}\left(\xi h_{ij}\xi^\dagger\right) T_{v\nu} \\
&\quad +2\mathcal{C}\left(\bar{T}_{v\mu}\left(\xi h_{ij}\xi^\dagger\right) B_v + \bar{B}_v\left(\xi h_{ij}\xi^\dagger\right) T_{v\mu}\right) \\
&\quad +if_\pi^2 \mathrm{Tr}\left(h_{ij}(\partial_\mu \Sigma^\dagger)\Sigma\right),
\end{aligned} \tag{2.5}$$

$$\mathcal{J}^{ij}_{(S+iP)} = \mathcal{J}^{ij}_{0(S+iP)} + \mathcal{J}^{ij}_{2(S+iP)} = \tag{2.6}$$

$$\begin{aligned}
\mathcal{J}^{ij}_{0(S+iP)} &= a_1 \mathrm{Tr}\bar{B}_v \left\{\xi^\dagger h_{ij}\xi^\dagger, B_v\right\} + a_2 \mathrm{Tr}\bar{B}_v \left[\xi^\dagger h_{ij}\xi^\dagger, B_v\right] \\
&\quad + a_3 \mathrm{Tr}\left(\bar{B}_v B_v\right) \mathrm{Tr}\left(\xi^\dagger h_{ij}\xi^\dagger\right) \\
&\quad + c_1 \bar{T}^\mu_v \left(\xi^\dagger h_{ij}\xi^\dagger\right) T_{v\mu} + c_2 \bar{T}^\mu_v T_{v\mu} \mathrm{Tr}\left(\xi^\dagger h_{ij}\xi^\dagger\right) \\
&\quad + \frac{f_\pi^2}{2} B_0 \mathrm{Tr}\left(h_{ij}\Sigma^\dagger\right)
\end{aligned} \tag{2.7}$$

$$\begin{aligned}
\mathcal{J}^{ij}_{2(S+iP)} &= 2B_0 L_4 \mathrm{Tr}\left(\mathcal{D}_\mu \Sigma \mathcal{D}^\mu \Sigma^\dagger\right) \mathrm{Tr}\left(h_{ij}\Sigma^\dagger\right) \\
&\quad + 2B_0 L_5 \mathrm{Tr}\left(h_{ij}\mathcal{D}_\mu \Sigma \mathcal{D}^\mu \Sigma^\dagger \Sigma^\dagger\right),
\end{aligned} \tag{2.8}$$

$$\mathcal{J}^{ij}_{(S-iP)} = \mathcal{J}^{ij}_{0(S-iP)} + \mathcal{J}^{ij}_{2(S-iP)} \tag{2.9}$$

$$\begin{aligned}
\mathcal{J}^{ij}_{0(S-iP)} &= a_1 \mathrm{Tr}\bar{B}_v \left\{\xi h_{ij}\xi, B_v\right\} + a_2 \mathrm{Tr}\bar{B}_v \left[\xi h_{ij}\xi, B_v\right] \\
&\quad + a_3 \mathrm{Tr}\left(\bar{B}_v B_v\right) \mathrm{Tr}\left(\xi h_{ij}\xi\right) \\
&\quad + c_1 \bar{T}^\mu_v \left(\xi h_{ij}\xi\right) T_{v\mu} + c_2 \bar{T}^\mu_v T_{v\mu} \mathrm{Tr}\left(\xi h_{ij}\xi\right) \\
&\quad + \frac{f_\pi^2}{2} B_0 \mathrm{Tr}\left(h_{ij}\Sigma\right)
\end{aligned} \tag{2.10}$$

$$\begin{aligned}
\mathcal{J}^{ij}_{2(S-iP)} &= 2B_0 L_4 \mathrm{Tr}\left(\mathcal{D}_\mu \Sigma \mathcal{D}^\mu \Sigma^\dagger\right) \mathrm{Tr}\left(h_{ij}\Sigma\right) \\
&\quad + 2B_0 L_5 \mathrm{Tr}\left(h_{ij}\mathcal{D}_\mu \Sigma \mathcal{D}^\mu \Sigma^\dagger \Sigma\right).
\end{aligned} \tag{2.11}$$

The flavor changing operator h_{ij} is given by

$$\left(h_{ij}\right)_{ab} = \begin{cases} 1 & a = i \text{ and } b = j \\ 0 & \text{others.} \end{cases} \tag{2.12}$$

In the following, we consider the effective weak Hamiltonian for the internal interaction.

2.2. Internal interaction

The diagram in Fig. 2.1(b) suggests that the interaction is described by the two point baryon vertex. And it has the operator changing the flavor $s \longrightarrow d$ for the $|\Delta S| = 1$ weak decay. Therefor the effective weak Hamiltonian of the internal interaction is the extension of the two point baryon vertex. And this Hamiltonian has the flavor changing operator h_{23} between the baryon operators. If the internal interaction Hamiltonian depends on the meson momentum, the lowest order of the weak vertex becomes the three point vertex constructed by the one meson and two baryon operators. We adopt only the momentum independent form for the internal interaction Hamiltonian in this study. The momentum dependent weak Hamiltonian is included in the current-current interaction.

The quark level effective weak Hamiltonian has six type operators, $O_1, \cdots, O_6$. If the internal interaction is considered outside the baryon, we can observe only the net flavor changing process $\left(\bar{d}s\right)$ and we cannot distinguish six operators. The internal interaction Hamiltonian, therefore, is described by the summation of the six operators. It is known that the weak interaction has only $V-A$ type symmetry[6]. This symmetry is represented by the transformation symmetry of the operator h_{23}. But in our method, Fierz transformation is applied to the quark level effective Hamiltonian, and the Hamiltonian includes the $(S \pm iP)$ symmetry mixing in operator O_{52}, O_{53}, O_{61} and O_{62} in eq.(2.1). Hence we consider the three types of the internal interaction Hamiltonian for the comparison. These Hamiltonians are given by

$$\mathcal{H}_{int}^{\Delta S=1} = \mathcal{H}_{int}^{min} \text{ or } \mathcal{H}_{int}^{V-A} \text{ or } \mathcal{H}_{int}^{S\pm iP} \tag{2.13}$$

$$\mathcal{H}_{int}^{min} = -\frac{G_f}{\sqrt{2}}\left(h_D \mathrm{Tr}\bar{B}_v\left\{h_{23}, B_v\right\} + h_F \mathrm{Tr} B_v\left[h_{23}, B_v\right] + h_C \bar{T}_v^{\mu}\left(h_{23}\right)T_{v\mu}\right) \tag{2.14}$$

$$\begin{aligned}\mathcal{H}_{int}^{V-A} = -\frac{G_f}{\sqrt{2}}\Big(& h_D \mathrm{Tr}\bar{B}_v\left\{\left(\xi^{\dagger}h_{23}\xi\right), B_v\right\} + h_F \mathrm{Tr} B_v\left[\left(\xi^{\dagger}h_{23}\xi\right), B_v\right] \\ & + h_C \bar{T}_v^{\mu}\left(\xi^{\dagger}h_{23}\xi\right)T_{v\mu} + h_M \mathrm{Tr}\left(\bar{B}_v B_v\right)\mathrm{Tr}\left(\xi^{\dagger}h_{23}\xi\right) + h_N \mathrm{Tr}\left(\bar{T}_v^{\mu}T_{v\mu}\right)\left(\xi^{\dagger}h_{23}\xi\right)\Big)\end{aligned} \tag{2.15}$$

$$\begin{aligned}\mathcal{H}_{int}^{S\pm iP} = -\frac{G_f}{\sqrt{2}}\Big(& h_{DS}\mathrm{Tr}\bar{B}_v\left\{\left(\xi h_{23}\xi + \xi^{\dagger}h_{23}\xi^{\dagger}\right), B_v\right\} + h_{FS}\mathrm{Tr}B_v\left[\left(\xi h_{23}\xi + \xi^{\dagger}h_{23}\xi^{\dagger}\right), B_v\right] \\ & + h_{MS}\mathrm{Tr}\left(\bar{B}_v B_v\right)\mathrm{Tr}\left(\xi h_{23}\xi + \xi^{\dagger}h_{23}\xi^{\dagger}\right) + h_{NS}\mathrm{Tr}\left(\bar{T}_v^{\mu}T_{v\mu}\right)\left(\xi h_{23}\xi + \xi^{\dagger}h_{23}\xi^{\dagger}\right) \\ & + h_{CS}\bar{T}_v^{\mu}\left(\xi h_{23}\xi + \xi^{\dagger}h_{23}\xi^{\dagger}\right)T_{v\mu} \\ & + h_{DP}\mathrm{Tr}\bar{B}_v\left\{\left(\xi h_{23}\xi - \xi^{\dagger}h_{23}\xi^{\dagger}\right), B_v\right\} + h_{FP}\mathrm{Tr}B_v\left[\left(\xi h_{23}\xi - \xi^{\dagger}h_{23}\xi^{\dagger}\right), B_v\right] \\ & + h_{MP}\mathrm{Tr}\left(\bar{B}_v B_v\right)\mathrm{Tr}\left(\xi h_{23}\xi - \xi^{\dagger}h_{23}\xi^{\dagger}\right) + h_{NP}\mathrm{Tr}\left(\bar{T}_v^{\mu}T_{v\mu}\right)\left(\xi h_{23}\xi - \xi^{\dagger}h_{23}\xi^{\dagger}\right) \\ & + h_{CP}\bar{T}_v^{\mu}\left(\xi h_{23}\xi - \xi^{\dagger}h_{23}\xi^{\dagger}\right)T_{v\mu}\Big).\end{aligned} \tag{2.16}$$

$\mathcal{H}_{int}^{min}$ has the minimum elements for the internal interaction and has three parameters h_D, h_F and h_C. $\mathcal{H}_{int}^{V-A}$ has the $V-A$ symmetry for the operator h_{23} and has five parameters. $\mathcal{H}_{int}^{S\pm iP}$ has the symmetry mixing $(S \pm iP)$ for the operator h_{23}. The number of parameters in this Hamiltonian is ten. In the following, using the effective weak Hamiltonian (2.1) and the strong interaction Lagrangian (1) in Appendix, we calculate hyperon non-leptonic weak decay amplitudes derived from the tree diagrams and the one-loop diagrams.

3. Result and Discussion

3.1. Numerical analysis

Ordinary non-leptonic weak decay amplitudes are represented by

$$\mathcal{M}(B_i \longrightarrow B_f + \pi) = G_F m_{\pi^+}^2 \bar{u}_f (A + B\gamma_5) u_i. \tag{3.1}$$

But the heavy baryon formalism of the chiral perturbation theory has the following expression

$$\mathcal{M}(B_i \longrightarrow B_f + \pi) = \frac{G_f}{\sqrt{2}} \bar{U}_f (\mathcal{A} + (q \cdot S_v)\mathcal{B}) U_i. \tag{3.2}$$

Hence we use the transformation equations

$$\begin{aligned} A &= \frac{-iG_f}{\sqrt{2}G_F m_{\pi^+}^2} f_\pi \mathcal{A} \\ B &= \frac{iG_f}{2\sqrt{2}G_F m_{\pi^+}^2} (E_f + m_f) f_\pi \mathcal{B}, \end{aligned} \tag{3.3}$$

and express the amplitudes in the ordinary form, which are also used in ref.[3]. The amplitudes are calculated in the tree level and the chiral logarithmic correction of the one-loop level with constants in Table 3.1. The computational method is the same as in ref.[3].

The parameters in the effective Hamiltonian are fitted by the experimental data and we can obtain hyperon weak decay amplitudes. In the experimental data, the number of independent data is eight. After the calculation of the diagrams, the current-current interaction Hamiltonian $\mathcal{H}_{current}^{|\Delta S|=1}$ has unknown parameters which are a_1, a_2, a_3 and c_1, and the numbers of unknown parameters in the internal interaction Hamiltonians $\mathcal{H}_{int}^{min}$, $\mathcal{H}_{int}^{V-A}$ and $\mathcal{H}_{int}^{S\pm iP}$ are 3, 3 and 7, respectively. Other parameters do not appear in the hyperon decay amplitudes. The parameter a_1 and a_2 that appear in the scalar current are determined as $a_1 = 29.1/m_s$ and $a_2 = -94.8/m_s$, where m_s is the strange quark mass. They are derived from the baryon mass difference with the chiral perturbation theory[7]. Therefor the effective weak Hamiltonian $\mathcal{H}_{current}^{|\Delta S|=1} + \mathcal{H}_{int}^{min}$ and $\mathcal{H}_{current}^{|\Delta S|=1} + \mathcal{H}_{int}^{V-A}$ have 5 unknown parameters. It is possible to determine them by the experimental data. But the effective Hamiltonian $\mathcal{H}_{current}^{|\Delta S|=1} + \mathcal{H}_{int}^{S\pm iP}$ has 9 unknown parameters and it is impossible to fix them exactly. In the following we take two steps to fix unknown parameters. First, introducing the assumption $h_{MP} = 0.0$, the remaining 8 parameters are fitted by the experimental data. Next, the parameter h_{MP} is fitted with 8 experimental data. It is not sure that this method gives the best fitted value for the decay amplitudes. In this study, our aim is not to obtain the exact value of the decay amplitudes, but is to obtain the parameter dependence of the amplitudes and the characteristic of the effective weak Hamiltonian.

After the parameter fitting, the obtained amplitudes and parameters are shown in Table 3.1 and Table 3.2, respectively. In these tables, the amplitudes $\mathcal{H}_{int}^{min}$ and $\mathcal{H}_{int}^{V-A(1)}$ are obtained by fitting 5 parameters in the effective weak Hamiltonian $\mathcal{H}_{current}^{|\Delta S|=1} + \mathcal{H}_{int}^{min}$ and $\mathcal{H}_{current}^{|\Delta S|=1} + \mathcal{H}_{int}^{V-A}$, respectively. The amplitudes $\mathcal{H}_{int}^{V-A(2)}$ are obtained by fitting 7 parameters in the effective weak Hamiltonian $\mathcal{H}_{current}^{|\Delta S|=1} + \mathcal{H}_{int}^{V-A}$, where the coupling constants a_1 and a_2 in the scalar and pseudo-scalar currents are also considered as unknown parameters. The amplitudes $\mathcal{H}_{int}^{S\pm iP}$ are obtained by fitting 9 parameters, applying the above assumptions. Table 3.2 suggests that the amplitudes $\mathcal{H}_{int}^{S\pm iP}$ and $\mathcal{H}_{int}^{V-A(2)}$ reproduce the experimental data well. In the following, we consider the amplitudes derived by $\mathcal{H}_{int}^{S\pm iP}$ and $\mathcal{H}_{int}^{V-A(2)}$. Table 3.4 and 3.5 show the components of the amplitudes derived by $\mathcal{H}_{int}^{S\pm iP}$ and $\mathcal{H}_{int}^{V-A(2)}$, respectively. The tree level amplitudes caused by each operators in eq. (2.1) are shown in Table 3.6 and 3.8. And the chiral logarithmic corrections caused by each operator are shown in Table 3.7 and 3.9.

3.2. DISCUSSION

It is known that the chiral perturbation theory cannot reproduce the experimental data of hyperon non-leptonic weak decay amplitudes[2]. The effective weak Hamiltonians in the previous study include the momentum independent baryon vertices, which correspond to the internal interaction Hamiltonian $\mathcal{H}_{int}^{V-A}$ in our analysis, and the momentum dependent meson weak vertices. Considering the products of the quark currents for the weak interaction, our effective Hamiltonian includes the momentum dependent baryon vertices and the effective Hamiltonian which depend on the scalar and pseudo-scalar currents. Our effective weak Hamiltonian is, therefore, the extension of the weak Hamiltonian in ref.[2]. Newly introduced terms have the same form as in ref.[8]. But our method have the constraints between the unknown parameters since we use the Noether currents to construct the effective weak Hamiltonian. In this paper we analyze the amplitudes caused by the internal interaction $\mathcal{H}_{int}^{V-A}$ and $\mathcal{H}_{int}^{S\pm iP}$ since they reproduce the experimental data quite well. The amplitudes derived by both Hamiltonians have the following characteristics.

1. It is large that the contribution of the chiral logarithmic correction in the one-loop graphs, which is shown in Table 3.4 and 3.5.
2. In the P-wave amplitudes, there are large cancelations between the amplitudes caused by the octet and the decuplet weak vertices in the logarithmic corrections.
3. In the chiral logarithmic corrections, there are cancelations between the amplitudes caused by the operators O_{61}, O_{62} and $\mathcal{H}_{int}^{|\Delta S|=1}$, which are shown in Table 3.7 and 3.9.

Our analysis suggests that the large cancelation improve the theoretical prediction of the decay amplitudes. And it is important to consider the effective weak Hamiltonian caused by the scalar and the pseudo-scalar currents.

Using the coupling constants a_1 and a_2 which derived by the baryon mass difference in the chiral perturbation theory, it is difficult to reproduce the experimental data with the internal interaction Hamiltonian $\mathcal{H}_{int}^{V-A}$, which corresponds to the amplitudes $\mathcal{H}_{int}^{V-A(1)}$ in Table 3.2. If the constants a_1 and a_2 are considered as unknown parameters and fitted by the experimentally obtained hyperon decay amplitudes, the parameter a_2 becomes more than zero, which are shown in Table 3.3, and it contradicts the calculation of the baryon masses. In order to adopt the effective weak Hamiltonian $\mathcal{H}_{current}^{|\Delta S|=1} + \mathcal{H}_{int}^{V-A}$ for the hyperon weak decay, we have to consider the derivation of the parameters a_1 and a_2.

4. Conclusion

Hyperon non-leptonic weak decays are analyzed with the chiral perturbation theory. For the weak interaction which happens inside the hyperon and cannot be described by the products of the hadronic currents, we introduce three types of the phenomenological weak Hamiltonian. One includes only the two point vertex of the baryon operators, and another includes $V-A$ type weak interaction and the other includes $S \pm iP$ type weak interaction. Our analysis suggests that the $V-A$ and the $S \pm iP$ type Hamiltonian can reproduce the experimental data fairly well. We can get the outlook that hyperon non-leptonic weak decay amplitudes can be represented by the chiral perturbation theory. But there remains the following three questions.

1. $S \pm iP$ type Hamiltonian looks like exceed the framework of the standard theory. How does it realize the $S \pm iP$ symmetry mixing in the weak interaction?
2. In the $V-A$ type Hamiltonian, the coupling constants a_1 and a_2 have the same sign, which contradict the sign derived by the baryon mass. What cause such a contradiction? How can we get the exact values of a_1 and a_2?
3. We use the constants in ref.[3] for the numerical analysis. There is an ambiguity in the quark condensation value B_0. In order to reproduce the experimental data exactly, the B_0 value has to be decided.

References

[1] J. Bijnens, H. Sonoda and M. B. Wise, Nucl. Phys. **B261** (1985) 185

[2] E. Jenkins, Nucl. Phys. **B375** (1992) 561
R. Springer, "Hyperon Decays in Chiral Perturbation Theory Revisited"
preprint DUKE-95-95

[3] K. Takayama and M. Oka, "Hyperon Non-leptonic Weak Decays in the Chiral Perturbation Theory I" hep-ph/9809388
K. Takayama, Thesis, Tokyo Institute of Technology 1997

[4] A. I. Valnshtein, V. I. Zakharov and M. A. Shifman JETP **45** ('77) 670
F. J. Gilman and M. B. Wise, Phys. Rev. **D20** (1979) 2392

[5] E. A. Paschos, T. Schneider and Y. L. Wu, Nucl. Phys. **B332** (1990) 285

[6] S. Weinberg, Phys. Rev. Lett. **19** (1967) 1264,
A. Salam : in Elementary Particle Theory ed. by N. Svartholom
D. Bailin, "Weak Interaction", (Adam Hilger LTD, Bristol, 1982)

[7] E. Jenkins, Nucl. Phys. **B368** (1992) 190

[8] B. Borasoy and B. R. Holstein, "Non-leptonic Hyperon Decays in Chiral Perturbation Theory" hep-ph/9805430

[9] E. Jenkins and A. V. Manohar, Phys. Lett. **B255** (1991) 558

[10] E. Jenkins and A. V. Manohar, Phys. Lett. **B259** (1991) 353

[11] J. Gasser and H. Leutwyler Ann. Phys. (N.Y.) **158** (1984) 142; Nucl. Phys. **B250** (1985) 465; Nucl. Phys. **B250** (1985) 517; Nucl. Phys. **B250** (1985) 539

[12] J. Bijnens and F. Cornet, Nucl. Phys. **B296** (1988) 557

[13] J. Bijnens, G. Ecker and J. Gasser, in :The DAFNE Physics Handbook (vol. 1),
eds. L. Maiani, G. Pancheri and N. Paver, INFN Frascati, 1992

Appendix. The Strong Interaction Lagrangian

The strong interaction Lagrangian in the heavy baryon formalism in the chiral perturbation theory is given by[9,10]

$$\begin{aligned}
\mathcal{L}_{strong} = & \frac{f_\pi^2}{4}\mathrm{Tr}\{(\mathcal{D}_\mu\Sigma)(\mathcal{D}^\mu\Sigma^\dagger) + \chi\Sigma^\dagger + \Sigma\chi^\dagger\} \\
& + i\mathrm{Tr}\bar{B}_v(v\cdot\mathcal{D})B_v + 2D\mathrm{Tr}\bar{B}_v S_v^\mu\{A_\mu, B_v\} + 2F\mathrm{Tr}\bar{B}_v S_v^\mu[A_\mu, B_v] \\
& - i\bar{T}_v^\mu(v\cdot\mathcal{D})T_{v\mu} + \mathcal{C}\left(\bar{T}_v^\mu A_\mu B_v + \bar{B}_v A_\mu T_v^\mu\right) + 2\mathcal{H}\bar{T}_v^\mu S_{v\nu}A^\nu T_{v\mu} \\
& + \Delta m\bar{T}_v^\mu T_{v\mu},
\end{aligned} \tag{1}$$

where A^μ, V^μ and $\mathcal{D}^\mu$ are represented by

$$\begin{aligned}
A^\mu &= \frac{i}{2}\left(\xi\partial^\mu\xi^\dagger - \xi^\dagger\partial^\mu\xi\right) \\
V^\mu &= \frac{1}{2}\left(\xi\partial^\mu\xi^\dagger + \xi^\dagger\partial^\mu\xi\right) \\
\mathcal{D}^\mu B_v &= \partial^\mu B_v + [V^\mu, B_v]\,.
\end{aligned}$$

Table 2.1 The values of the coefficients in the effective weak Hamiltonian (2.2). The values are taken from ref.[5]. The data set 1 corresponds to the choices $m_t = 200$[GeV] and $\mu_0 = 0.24$[GeV], $\Lambda_{QCD} = 0.10$. The data set 2 corresponds to the choices $m_t = 200$[GeV] and $\mu_0 = 0.71$[GeV], $\Lambda_{QCD} = 0.316$. In both cases, μ_0 is defined so as to satisfy $\alpha_s(\mu^2) = 1$.

	data set 1	data set 2
μ(GeV)	0.24	0.71
$\Lambda^{(4)}$(GeV)	0.10	0.316
K_1	-0.284	-0.270
K_2	0.009	0.011
K_3	0.026	0.027
K_4	0.026	0.027
K_5	0.004	0.002
K_6	0.004	0.002

Table 3.1 Hadron masses and coupling constants used in the numerical analysis of the hyperon decay amplitudes. m, M and f_π correspond to the baryon mass, the meson mass and pion decay constant, respectively. Phenomenological coupling constants $\mathcal{D}$, $\mathcal{F}$ and $\mathcal{H}$ are taken from ref.[9,10]. The renormalized coupling constants L_4 and L_5 are taken from ref.[11], where the renormalization scale $4\pi\mu^2 = 1.0 \times 10^6[\mathrm{MeV}^2]$ is used. The constant B_0 corresponds to the quark condensation value which is changed for the hyperon decay amplitudes[3].

$$\begin{array}{rcc rcc rcc}
m_n & = & 939[\mathrm{MeV}], & m_\Sigma & = & 1193[\mathrm{MeV}], & m_\Lambda & = & 1116[\mathrm{MeV}] \\
m_\Xi & = & 1318[\mathrm{MeV}], & m_\Delta & = & 1232[\mathrm{MeV}], & m_{\Sigma^*} & = & 1385[\mathrm{MeV}] \\
m_{\Xi^*} & = & 1533[\mathrm{MeV}], & m_\Omega & = & 1672[\mathrm{MeV}] & & & \\
M_\pi & = & 138[\mathrm{MeV}], & M_K & = & 496[\mathrm{MeV}], & M_\eta & = & 547[\mathrm{MeV}] \\
D & = & 0.61, & F & = & 0.40, & \mathcal{C} & = & 1.6 \\
\mathcal{H} & = & -1.9, & f_\pi & = & 93[\mathrm{Mev}], & L_4 & = & -0.3003 \\
L_5 & = & 1.399, & B_0 & = & 139.14[\mathrm{MeV}], & & &
\end{array}$$

Table 3.2 The tree and one-loop level amplitudes. Second column corresponds the experimentally obtained data. Two types of the data set which is shown in Table 2.1 are used for the calculation of the S- and P-wave amplitudes.

S-wave:data set 1

process	exp.	$\mathcal{H}_{int}^{min}$	$\mathcal{H}_{int}^{V-A(1)}$	$\mathcal{H}_{int}^{V-A(2)}$	$\mathcal{H}_{int}^{S\pm iP}$
Σ^-_-	1.93 ± 0.01	5.803	5.124	2.486	2.469
Σ^+_+	0.06 ± 0.01	-0.1616	-0.1537	-0.1609	-0.1838
Σ^+_0	-1.48 ± 0.05	-2.276	-2.540	-0.6831	-0.7049
Λ^0_0	-1.07 ± 0.02	0.9174	0.1827	-0.4942	-0.4723
Λ^0_-	1.47 ± 0.01	0.6009	0.9013	1.875	1.883
Ξ^-_-	-2.04 ± 0.01	-5.674	-4.649	-2.543	-2.544
Ξ^0_0	1.54 ± 0.03	2.089	2.338	0.8412	0.8338

S-wave:data set 2

process	exp.	$\mathcal{H}_{int}^{min}$	$\mathcal{H}_{int}^{V-A(1)}$	$\mathcal{H}_{int}^{V-A(2)}$	$\mathcal{H}_{int}^{S\pm iP}$
Σ^-_-	1.93 ± 0.01	3.053	3.455	2.467	2.460
Σ^+_+	0.06 ± 0.01	-0.09894	-0.09483	-0.09799	-0.1041
Σ^+_0	-1.48 ± 0.05	-1.124	-1.405	-0.7102	-0.7155
Λ^0_0	-1.07 ± 0.02	-0.2427	-0.2096	-0.4784	-0.4669
Λ^0_-	1.47 ± 0.01	1.555	1.499	1.887	1.886
Ξ^-_-	-2.04 ± 0.01	-3.152	-3.393	-2.535	-2.534
Ξ^0_0	1.54 ± 0.03	1.288	1.463	0.8527	0.8478

P-wave:data set 1

process	exp.	$\mathcal{H}_{int}^{min}$	$\mathcal{H}_{int}^{V-A(1)}$	$\mathcal{H}_{int}^{V-A(2)}$	$\mathcal{H}_{int}^{S\pm iP}$
Σ^-_-	-0.65 ± 0.07	1.400	0.8779	0.8624	0.8623
Σ^+_+	19.07 ± 0.07	17.02	17.50	17.56	17.56
Σ^+_0	12.04 ± 0.58	14.94	14.12	14.18	14.18
Λ^0_0	-7.14 ± 0.56	-9.935	-7.240	-7.237	-7.237
Λ^0_-	9.98 ± 0.24	8.004	9.922	9.912	9.912
Ξ^-_-	6.93 ± 0.31	8.796	7.565	7.569	7.567
Ξ^0_0	-6.43 ± 0.66	-3.792	-5.507	-5.526	-5.529

P-wave:data set 2

process	exp.	$\mathcal{H}_{int}^{min}$	$\mathcal{H}_{int}^{V-A(1)}$	$\mathcal{H}_{int}^{V-A(2)}$	$\mathcal{H}_{int}^{S\pm iP}$
Σ^-_-	-0.65 ± 0.07	0.8957	0.9010	0.8955	0.8957
Σ^+_+	19.07 ± 0.07	17.52	17.50	17.52	17.52
Σ^+_0	12.04 ± 0.58	14.23	14.20	14.23	14.23
Λ^0_0	-7.14 ± 0.56	-7.250	-7.251	-7.250	-7.250
Λ^0_-	9.98 ± 0.24	9.902	9.906	9.903	9.902
Ξ^-_-	6.93 ± 0.31	7.566	7.568	7.570	7.566
Ξ^0_0	-6.43 ± 0.66	-5.530	-5.518	-5.525	-5.530

Table 3.3 Parameters in the scalar and pseudo-scalar currents and in the internal interaction Hamiltonian. Two types of data set are used for the parameter fitting. The parameters are fitted with least square method for each effective Hamiltonian.

$\mathcal{H}_{int}^{min}$

parameter	data set 1	data set 2
h_D	-2.1603E-1	-1.5271E-1
h_F	4.4585E-1	2.8016E-1
h_C	1.7336E 1	1.1714E 1
a_1	1.9400E-1	1.9400E-1
a_2	-6.3200E-1	-6.3200E-1
a_3	4.0329E 1	5.8615E 1
c_1	1.0971E 2	1.0023E 2

$\mathcal{H}_{int}^{V-A(1)}$

parameter	data set 1	data set 2
h_D	-2.4929E-1	-1.9314E-1
h_F	5.1938E-1	2.6855E-1
h_C	1.0896E 1	8.4955
a_1	1.9400E-1	1.9400E-1
a_2	-6.3200E-1	-6.3200E-1
a_3	-3.3276	-3.6489
c_1	-1.0240E 2	-2.5716E 2

$\mathcal{H}_{int}^{V-A(2)}$

parameter	data set 1	data set 2
h_D	-8.6476E-2	-1.4807E-1
h_F	1.1019E-2	4.5324E-2
h_C	1.0839E 1	8.7308
a_1	6.2889E-2	1.6273E-1
a_2	8.6041E-2	3.6301E-2
a_3	-9.4523	-9.0925
c_1	-2.4254E 2	-4.0113E 2

$\mathcal{H}_{int}^{S\pm iP}$

parameter	data set 1	data set 2
h_{DS}	-1.4405E-1	-1.3792E-1
h_{FS}	2.9850E-1	2.0563E-1
h_{CS}	5.7787	4.7978
h_{DP}	-1.2303E-1	-6.4850E-3
h_{FP}	6.3642E-1	2.6492E-1
h_{CP}	-1.4015	-1.1624
h_{MP}	3.7366E-1	4.0328E-1
a_1	1.9400E-1	1.9400E-1
a_2	-6.3200E-1	-6.3200E-1
a_3	-1.5603	6.4024
c_1	-7.5060E 1	-1.1388E 2

Table 3.4 The predicted amplitudes with the effective weak Hamiltonian $\mathcal{H}^{|\Delta S|=1}_{current} + \mathcal{H}^{S\pm iP}_{int}$, data set 1 and the parameters in Table 3.2. A_{exp} and B_{exp} correspond to the experimental data. A_{tree} and B_{tree} are the tree level amplitudes. ΔA_{loop} and ΔB_{loop} are the summation of the chiral logarithmic corrections of the one-loop graphs. They are represented by $\Delta A_{loop} = \Delta A_{octet} + \Delta A_{decuplet}$ and $\Delta B_{loop} = \Delta B_{octet} + \Delta B_{decuplet}$. A_{theory} and B_{theory} are the total amplitude of the chiral perturbation theory, which are represented by $A_{theory} = A_{tree} + \Delta A_{loop}$ and $B_{theory} = B_{tree} + \Delta B_{loop}$.

S-wave:

decay mode	$A_{exp.}$	A_{theory}	A_{tree}	ΔA_{loop}	ΔA_{octet}	$\Delta A_{decuplet}$
Σ^-_-	1.93 ± 0.01	2.469	-0.4684	2.937	2.905	0.03211
Σ^+_+	0.06 ± 0.01	-0.1838	0.0	-0.1838	-0.06445	-0.1193
Σ^+_0	-1.48 ± 0.05	-0.7049	0.4723	-1.177	-1.964	0.7863
Λ^0_0	-1.07 ± 0.02	-0.4723	0.4571	-0.9293	-0.7257	-0.2036
Λ^0_-	1.47 ± 0.01	1.883	-0.4680	2.351	1.724	0.6277
Ξ^-_-	-2.04 ± 0.01	-2.544	0.5362	-3.080	-3.053	-0.02747
Ξ^-_0	1.54 ± 0.03	0.8338	-0.5217	1.356	1.909	-0.5536

P-wave:

decay mode	$B_{exp.}$	B_{theory}	B_{tree}	ΔB_{loop}	ΔB_{octet}	$\Delta B_{decuplet}$
Σ^-_-	-0.65 ± 0.07	0.8623	0.9363	-0.07397	12.05	-12.13
Σ^+_+	19.07 ± 0.07	17.56	5.996	11.56	-12.37	23.93
Σ^+_0	12.04 ± 0.58	14.18	3.857	10.32	-16.95	27.27
Λ^0_0	-7.14 ± 0.56	-7.237	-2.674	-4.563	45.35	-49.92
Λ^0_-	9.98 ± 0.24	9.912	2.401	7.511	-65.16	72.67
Ξ^-_-	6.93 ± 0.31	7.567	-1.341	8.909	26.63	-17.72
Ξ^-_0	-6.43 ± 0.66	-5.529	1.327	-6.856	-18.20	11.35

Table 3.5 The predicted amplitudes with the effective weak Hamiltonian $\mathcal{H}^{|\Delta S|=1}_{current}+\mathcal{H}^{V-A(2)}_{int}$ and data set 1. A_{exp} and B_{exp} correspond to the experimental data. A_{tree} and B_{tree} are the tree level amplitudes. ΔA_{loop} and ΔB_{loop} are the summation of the chiral logarithmic corrections of the one-loop graphs. They are represented by $\Delta A_{loop} = \Delta A_{octet} + \Delta A_{decuplet}$ and $\Delta B_{loop} = \Delta B_{octet} + \Delta B_{decuplet}$. A_{theory} and B_{theory} are the total amplitude of the chiral perturbation theory, which are represented by $A_{theory} = A_{tree} + \Delta A_{loop}$ and $B_{theory} = B_{tree} + \Delta B_{loop}$.

S-wave:

decay mode	$A_{exp.}$	A_{theory}	A_{tree}	ΔA_{loop}	ΔA_{octet}	$\Delta A_{decuplet}$
Σ^-_-	1.93 ± 0.01	3.455	0.05723	3.398	1.938	1.460
Σ^+_+	0.06 ± 0.01	-0.09483	0.0	-0.09483	-0.04009	-0.05474
Σ^+_0	-1.48 ± 0.05	-1.405	0.1061	-1.511	-1.287	-0.2243
Λ^0_0	-1.07 ± 0.02	-0.2096	0.03464	-0.2442	-0.8104	0.5662
Λ^0_-	1.47 ± 0.01	1.499	0.1363	1.363	1.809	-0.4460
Ξ^-_-	-2.04 ± 0.01	-3.393	-0.08803	-3.305	-1.972	-1.332
Ξ^-_0	1.54 ± 0.03	1.463	-0.08577	1.548	1.178	0.3707

P-wave:

decay mode	$B_{exp.}$	B_{theory}	B_{tree}	ΔB_{loop}	ΔB_{octet}	$\Delta B_{decuplet}$
Σ^-_-	-0.65 ± 0.07	0.9010	0.5866	0.3144	3.365	-3.051
Σ^+_+	19.07 ± 0.07	17.50	3.079	14.42	-5.204	19.63
Σ^+_0	12.04 ± 0.58	14.20	2.053	12.15	-5.727	17.88
Λ^0_0	-7.14 ± 0.56	-7.251	-1.001	-6.250	17.86	-24.11
Λ^0_-	9.98 ± 0.24	9.906	-0.01803	9.925	-26.34	36.26
Ξ^-_-	6.93 ± 0.31	7.568	0.06998	7.498	11.24	-3.737
Ξ^-_0	-6.43 ± 0.66	-5.518	0.3436	-5.862	-7.270	1.409

Table 3.6 The amplitudes for each operator in the tree level calculation with the effective weak Hamiltonian $\mathcal{H}^{|\Delta S|=1}_{current} + \mathcal{H}^{S\pm iP}_{int}$ and data set 1. The first column corresponds to the operator types of the effective Hamiltonian (2.2) and (2.16). The second row shows the experimentally obtained data.

S-wave:

vertex	Σ^-_-	Σ^+_+	Σ^+_0	Λ^0_0	Λ^0_-	Ξ^-_-	Ξ^-_0
exp.	1.93	0.06	-1.48	-1.07	1.47	-2.04	-1.54
O_1	0.2180	0.0	-0.1542	-0.1378	0.1949	-0.2202	0.1557
O_2	0.01382	0.0	-0.009770	-0.008735	0.01235	-0.01396	0.009868
O_3	0.01331	0.0	-0.009408	-0.008411	0.01190	-0.01344	0.009502
O_4	0.06653	0.0	0.09408	0.08411	0.05948	-0.06719	-0.09502
O_{51}	0.0	0.0	0.0	0.0	0.0	0.0	0.0
O_{52}	0.0007510	0.0	-0.0005311	-0.0004467	0.0006318	-0.0007758	0.0005486
O_{53}	0.0	0.0	0.0	0.0	0.0	0.0	0.0
O_{61}	-0.02103	0.0	0.01487	0.01251	-0.01769	0.02172	-0.01536
O_{62}	0.0	0.0	0.0	0.0	0.0	0.0	0.0
$\mathcal{H}^{S\pm iP}_{int}$	-0.7598	0.0	0.5372	0.5159	-0.7295	0.8300	-0.5869

P-wave:

vertex	Σ^-_-	Σ^+_+	Σ^+_0	Λ^0_0	Λ^0_-	Ξ^-_-	Ξ^-_0
exp.	-0.65	19.07	12.04	-7.14	9.98	6.93	-6.43
O_1	0.4317	0.0	-0.3053	1.066	-1.508	0.5847	-0.4135
O_2	0.02736	0.0	-0.01935	0.06759	-0.09559	0.03706	-0.02621
O_3	0.02635	0.0	-0.01863	0.06509	-0.09205	0.03569	-0.02523
O_4	0.1317	0.0	0.1863	-0.6509	-0.4602	0.1784	0.2523
O_{51}	0.0	0.0	0.0	0.0	0.0	0.0	0.0
O_{52}	0.001240	0.01128	0.007101	-0.006488	0.009176	-0.005211	0.003685
O_{53}	-0.001368	0.0	0.0009674	-0.003380	0.004779	-0.001853	0.001310
O_{61}	-0.03472	-0.3159	-0.1988	0.1817	-0.2569	0.1459	-0.1032
O_{62}	0.03831	0.0	-0.02709	0.09463	-0.1338	0.05188	-0.03669
$\mathcal{H}^{S\pm iP}_{int}$	0.3157	6.301	4.232	-3.489	4.934	-2.368	1.675

Table 3.7 The amplitudes for each operator, which are derived from the one-loop calculation with the effective weak Hamiltonian $\mathcal{H}^{|\Delta S|=1}_{current} + \mathcal{H}^{S\pm iP}_{int}$ and data set 1. The first column corresponds to the operator types of the effective Hamiltonian (2.2) and (2.16). The second row shows the experimentally obtained data.

S-wave:

vertex	Σ^-_-	Σ^+_+	Σ^+_0	Λ^0_0	Λ^0_-	Ξ^-_-	Ξ^-_0
exp.	1.93	0.06	-1.48	-1.07	1.47	-2.04	-1.54
O_1	0.8530	0.03913	-0.5675	-0.8295	1.182	-1.275	0.9032
O_2	0.05406	0.002480	-0.03597	-0.05257	0.07492	-0.08080	0.05724
O_3	0.1296	0.004146	-0.08691	-0.05800	0.08250	-0.1622	0.1134
O_4	0.3841	-0.07977	0.4795	0.4600	0.3195	-0.3399	-0.4790
O_{51}	0.0	0.0	0.0	0.0	0.0	0.0	0.0
O_{52}	-0.01267	0.00001678	0.008974	0.05773	-0.08168	0.02882	-0.02036
O_{53}	-0.1266	0.004708	0.08431	0.06087	-0.08676	0.1230	-0.08344
O_{61}	0.3548	-0.0004700	-0.2513	-1.616	2.287	-0.8070	0.5701
O_{62}	3.545	-0.1318	-2.361	-1.704	2.429	-3.444	2.336
$\mathcal{H}^{S\pm iP}_{int}$	-2.244	-0.02220	1.552	2.753	-3.856	2.877	-2.042

P-wave:

vertex	Σ^-_-	Σ^+_+	Σ^+_0	Λ^0_0	Λ^0_-	Ξ^-_-	Ξ^-_0
exp.	-0.65	19.07	12.04	-7.14	9.98	6.93	-6.43
O_1	0.5927	7.247	4.705	-1.630	2.305	0.008264	-0.005844
O_2	0.04233	0.4647	0.2987	-0.1014	0.1434	0.004622	-0.003268
O_3	0.06285	-0.2282	-0.2058	0.1922	-0.2718	-0.1290	0.09123
O_4	0.9896	-0.004056	1.397	0.4862	0.3438	-0.2587	-0.3658
O_{51}	-7.953E-4	-8.974E-4	-7.224E-5	-3.121E-4	4.414E-4	-6.831E-4	4.830E-4
O_{52}	-0.8894	-0.3386	0.3895	-1.813	2.564	-1.055	0.7461
O_{53}	0.1745	0.7492	0.4066	-0.3720	0.5251	-0.3250	0.2301
O_{61}	24.90	9.480	-10.91	50.76	-71.79	29.55	-20.89
O_{62}	-4.885	-20.98	-11.39	10.42	-14.70	9.100	-6.443
$\mathcal{H}^{S\pm iP}_{int}$	-21.06	15.17	25.62	-62.50	88.39	-27.98	19.79

Table 3.8 The amplitudes for each operator in the tree level calculation with the effective weak Hamiltonian $\mathcal{H}^{|\Delta S|=1}_{current} + \mathcal{H}^{V-A}_{int}$ and data set 1. The first column corresponds to the operator types of the effective Hamiltonian (2.2) and (2.15). The second row shows the experimentally obtained data.

S-wave:

vertex	Σ^-_-	Σ^+_+	Σ^+_0	Λ^0_0	Λ^0_-	Ξ^-_-	Ξ^-_0
exp.	1.93	0.06	-1.48	-1.07	1.47	-2.04	-1.54
O_1	0.2180	0.0	-0.1542	-0.1378	0.1949	-0.2202	0.1557
O_2	0.01382	0.0	-0.009770	-0.008735	0.01235	-0.01396	0.009868
O_3	0.01331	0.0	-0.009408	-0.008411	0.01190	-0.01344	0.009502
O_4	0.06653	0.0	0.09408	0.08411	0.05948	-0.06719	-0.09502
O_{51}	0.0	0.0	0.0	0.0	0.0	0.0	0.0
O_{52}	-2.105E-5	0.0	1.489E-5	8.426E-5	-1.192E-4	7.247E-5	-5.124E-5
O_{53}	0.0	0.0	0.0	0.0	0.0	0.0	0.0
O_{61}	0.0005894	0.0	-0.0004168	-0.002359	0.003336	-0.002029	0.001435
O_{62}	0.0	0.0	0.0	0.0	0.0	0.0	0.0
$\mathcal{H}^{V-A}_{int}$	-0.05072	0.0	0.03587	-0.008023	0.01135	0.02539	-0.01795

P-wave:

vertex	Σ^-_-	Σ^+_+	Σ^+_0	Λ^0_0	Λ^0_-	Ξ^-_-	Ξ^-_0
exp.	-0.65	19.07	12.04	-7.14	9.98	6.93	-6.43
O_1	0.4317	0.0	-0.3053	1.066	-1.508	0.5847	-0.4135
O_2	0.02736	0.0	-0.01935	0.06759	-0.09559	0.03706	-0.02621
O_3	0.02635	0.0	-0.01863	0.06509	-0.09205	0.03569	-0.02523
O_4	0.1317	0.0	0.1863	-0.6509	-0.4602	0.1784	0.2523
O_{51}	0.0	0.0	0.0	0.0	0.0	0.0	0.0
O_{52}	-4.622E-4	-8.578E-4	-2.797E-4	1.235E-3	-1.746E-3	1.528E-3	-1.080E-3
O_{53}	-0.001368	0.0	0.0009674	-0.003380	0.004779	-0.001853	0.001310
O_{61}	0.01294	0.02402	0.007832	-0.03457	0.04890	-0.04278	0.03025
O_{62}	0.03831	0.0	-0.02709	0.09463	-0.1338	0.05188	-0.03669
$\mathcal{H}^{V-A}_{int}$	-0.2121	0.4736	0.4848	-0.04624	0.06539	0.2913	-0.2060

Table 3.9 The amplitudes for each operator, which are derived from the one-loop calculation with the effective weak Hamiltonian $\mathcal{H}_{current}^{|\Delta S|=1} + \mathcal{H}_{int}^{V-A}$ and data set 1. The first column corresponds to the operator types of the effective Hamiltonian (2.2) and (2.15). The second row shows the experimentally obtained data.

S-wave:

vertex	Σ^-_-	Σ^+_+	Σ^+_0	Λ^0_0	Λ^0_-	Ξ^-_-	Ξ^-_0
exp.	1.93	0.06	-1.48	-1.07	1.47	-2.04	-1.54
O_1	0.8530	0.03913	-0.5675	-0.8295	1.182	-1.275	0.9032
O_2	0.05406	0.002480	-0.03597	-0.05257	0.07492	-0.08080	0.05724
O_3	0.1296	0.004146	-0.08691	-0.05800	0.08250	-0.1622	0.1134
O_4	0.3841	-0.07977	0.4795	0.4600	0.3195	-0.3399	-0.4790
O_{51}	0.0	0.0	0.0	0.0	0.0	0.0	0.0
O_{52}	-0.04769	-2.247	0.03372	0.1913	-0.2706	0.1004	-0.07101
O_{53}	-0.02115	0.004708	0.009744	-0.01165	0.01580	0.007148	-0.001518
O_{61}	1.335	0.00006291	-0.9442	-5.357	7.576	-2.812	1.988
O_{62}	0.5923	-0.1318	-0.2728	0.3262	-0.4424	-0.2001	0.04251
$\mathcal{H}_{int}^{V-A}$	-1.055	0.0001877	0.7451	4.919	-6.956	2.511	-1.776

P-wave:

vertex	Σ^-_-	Σ^+_+	Σ^+_0	Λ^0_0	Λ^0_-	Ξ^-_-	Ξ^-_0
exp.	-0.65	19.07	12.04	-7.14	9.98	6.93	-6.43
O_1	0.5927	7.247	4.705	-1.630	2.305	0.008264	-0.005844
O_2	0.04233	0.4647	0.2987	-0.1014	0.1434	0.004622	-0.003268
O_3	0.06285	-0.2282	-0.2058	0.1922	-0.2718	-0.1290	0.09123
O_4	0.9896	-0.004056	1.397	0.4862	0.3438	-0.2587	-0.3658
O_{51}	-7.953E-4	-8.974E-4	-7.224E-5	-3.121E-4	4.414E-4	-6.831E-4	4.830E-4
O_{52}	-1.617	-1.384	0.1645	-2.453	3.469	-1.508	1.067
O_{53}	0.6537	-0.1189	-0.5461	1.436	-2.032	0.9439	-0.6671
O_{61}	45.27	38.76	-4.605	68.69	-97.14	42.24	-29.87
O_{62}	-18.30	3.329	15.29	-40.22	56.90	-26.43	18.68
$\mathcal{H}_{int}^{V-A}$	-27.28	-31.00	-2.629	-34.20	48.36	-8.436	5.969

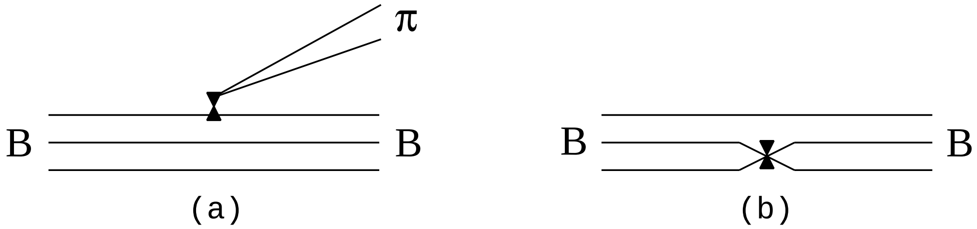

Figure 2.1: $\Delta S = 1$ hyperon non-leptonic weak decay diagrams of quark currents. (a) corresponds to the weak interaction between two hadronic currents which are color singlet. (b) corresponds to the weak interaction inside the hyperon.